IEICE TRANS. FUNDAMENTALS, VOL.E90–A, NO.3 MARCH 2007

PAPER

Equivalent Parallel Structure of Deinterlacer Banks and Its Application to Optimal Bit-Rate Allocation

Minoru HIKI[†a)], ***Student Member***, **Shogo MURAMATSU**[†], **Takuma ISHIDA**[††], ***Members***, ***and*** **Hisakazu KIKUCHI**[†], ***Fellow***

SUMMARY In this paper, theoretical properties of deinterlacer banks are analyzed. Deinterlacer banks are novel filter banks in the sense that a progressive video sequence is separated into two progressive video sequences of a half frame rate and, furthermore, interlaced sequences are produced as intermediate data. Unlike the conventional filter banks, our deinterlacer banks are constructed in a way unique to multidimensional systems by using invertible deinterlacers, which the authors have proposed before. The system is a kind of shift-varying filter banks and it was impossible to derive the optimal bit-allocation control without any equivalent parallel filter banks. This paper derives an equivalent polyphase matrix representation of the whole system and its equivalent parallel structure, and then shows the optimal rate allocation for the deinterlacer banks. Some experimental results justify the effectiveness of the optimal rate allocation through our theoretical analysis.

key words: *3-D filter banks, scalable video coding, rate-distortion control, interlace video*

1. Introduction

The ideal goal of scalable video compression is to encode a video once and then partially decode the bit-stream through truncation at a lower bit-rate, spatial resolution and/or frame rate in the best possible quality as if it had been optimized to each decoding condition. Network video applications such as interactive video library and Internet video streaming require rate control over a wide range of bit-rates because there must be various kinds of terminals, and channel bandwidth for each terminal changes largely moment by moment. Scalable video coding achieves this control simply by truncating the bit-streams after the source has been compressed.

Recent developments in such video coding aim at providing fine granular control of quality, frame-rate and resolution to meet the requirements of end users. Most of them employ 3-D wavelet-based techniques with motion compensation, in which motion compensated temporal filtering (MCTF) is performed. For the spatio-temporal scalability, filter banks and discrete wavelet transforms (DWT) play an important role in scalable video coding [1]–[3]. In the article [1], the use of a separable 3-D DWT for video compression was first proposed. In the articles [2], [3], a 3-D lifting DWT scheme with MCTF is introduced, in which a spatio-temporal transform precedes embedded quantization and bit-plane coding as done in the current state-of-the-art scalable codec for still pictures, namely JPEG2000 [4].

So far, there have been only two choices of the spatio-temporal resolution control with respect to video formats. One is to handle a video only in the progressive scanning manner [2], and the other is to divide a video into an interlaced or non-rectangular sampled field sequence and its residual [5]. The former can achieve a finer scalability through multi-stage tree-structured filter banks. In contrast, the latter is not suitable for such frameworks since the subband signals are not in the same progressive manner as the input. However, the interlaced subband signals have an advantage of the preservation of update temporal interval with reduced frame rate.

As previous works, we constructed perfect reconstruction (PR) deinterlacer banks by using invertible deinterlacers as new tools for spatio-temporal scalable video codec [6]–[11]. Our deinterlacer banks also belong to the MCTF category. The deinterlacer banks, however, enjoy a definitely different function from others with respect to handling of video formats, where the vertical-temporal (VT) quincunx and face-centered orthorhombic (FCO) format are dealt with. Furthermore, the reconstruction of the original full frame-rate progressive video is guaranteed by the PR property. The deinterlacer banks provides an interlaced sequence as intermediate data, a half-rate progressive sequence, as well as the original rate video sequence. That is, the deinterlacer banks give a new spatio-temporal scalable function, which we refer to as *Field Scalability*. In the article [8], as a primal application of the single stage motion-compensated deinterlacer banks, a simple two-layer field scalable video codec system using JPEG2000 was experimented. In the articles [10], [11], the multi-stage deinterlacer banks are developed for fine spatio-temporal multiresolution control. However, in those works, gain compensation for optimal bit-rate allocation through theoretical analysis of deinterlacer banks was not taken into account. This is become the deinterlacer banks are shift-varying and it was impossible to derive optimal bit-rate allocation without knowing coefficients of analysis and synthesis filters in the equivalent parallel structure.

In this paper, to make the optimal bit-rate allocation

Manuscript received November 10, 2005.
Manuscript revised August 2, 2006.
Final manuscript received November 20, 2006.

[†]The authors are with the Department of Electrical and Electronic Engineering, Niigata University, Niigata-shi, 950-2181 Japan.
[††]The author is with Product Development Department, NETCLEUS Systems Corporation, Fujisawa-shi, 251-0052 Japan.
a) E-mail: mhiki@telecom0.eng.niigata-u.ac.jp

DOI: 10.1093/ietfec/e90–a.3.642

possible, we theoretically analyze the deinterlacer banks, and derive the equivalent parallel structures. Some experimental results show the effectiveness of optimal rate allocation given our theoretical analysis. The organization of this paper is as follows: Sect. 2 reviews interlaced scanning and deinterlacer banks dealt with in this work. Section 3 discusses the polyphase representation of the deinterlacer banks and its equivalent parallel structure. Section 4 evaluates the performance of the deinterlacer banks and justifies the significance of our theoretical analysis. Then, conclusions follow in Sect. 5. For the sake of convenience, Appendix A summarizes the notations used throughout this paper.

2. Review of PR Deinterlacer Banks

As a preliminary, deinterlacer banks are reviewed, and two types of interlaced sampling formats are introduced in this section.

2.1 Deinterlacer Banks [8]

The deinterlacer banks decompose a progressive video into two subband sequences of a half frame-rate in the progressive scanning manner. Even though the system handles interlaced videos as intermediate data, introducing a multi-stage decomposition is simply achieved because the output sequences have also the progressive format as like the input. Unlike other filter banks [1], [2], [12], our deinterlacer banks are constructed in a way unique to multi-dimensional systems by using invertible deinterlacers, which are regarded as 1-ch filter banks [6]. Figure 1 shows a single stage structure of a pair of deinterlacer and reinterlacer bank. The deinterlacer bank shown in Fig. 1(a) is composed of a field splitter, two invertible deinterlacers, and a frame predictor. The deinterlacer bank separates an input frame sequence $x(n)$ into two different frames $y_0(k)$ and $y_1(k)$ of a half frame rate, where disagreeable artifacts such as comb-tooth and dot-pattern artifacts, which cause in the field split process, are suppressed beforehand by the invertible deinterlacers. Frame sequence $y_1(k)$ is given as prediction errors so as to exploit the temporal redundancy. The frame predictor is exactly the same operation as the prediction step of lifting wavelet. Existing lifting-based MCTF schemes consist of a frame split, prediction and update step with motion compensation for the temporal decomposition. In our deinterlacer banks, the field split process takes the place of the frame split process. Additionally, our structure removes the update operation to avoid complex calculation and ghosting artifacts in subband $y_0(k)$. Indeed, the main reason is that recovering field sequence $q(k)$ becomes possible only from the temporal-low subband sequence.

The inverse transform is shown in Fig. 1(b), namely reinterlacer bank, where 'Field Mer.' denotes field merge process, which is the inverse process of the field split process. Note that the structure shown in Fig. 1 resembles to the 1/3 transform presented in the LIMAT framework [2], and any motion compensation technique can be applied to the frame prediction.

The sampling lattice alteration with sampling density preservation is meaningless in one dimension. Thus, the problem to be considered is worth discussing only in the multidimensional case. Invertible deinterlacers are multidimensional shift-varying systems, and regarded as 1-ch filter banks. Deinterlacer banks composed of invertible deinterlacers, therefore, had a problem in allocating bits to subbands. In the next section, equivalent parallel structure of deinterlacer banks will be derived to make the conventional optimal bit-rate allocation available.

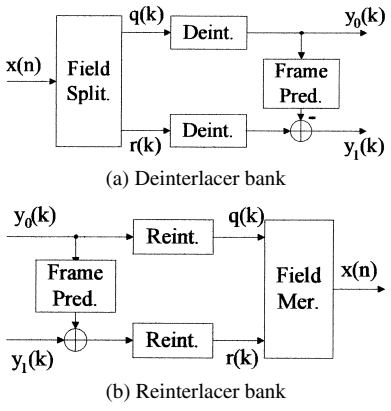

Fig. 1 Structures of deinterlacer banks and its inverse.

2.2 Sub-Sampling Format

In this paper, two types of field sequences are used: the popular VT-quincunx and FCO format. Figure 2 summarizes both of the video formats. This paper refers to the sequence as shown in Fig. 2(a) as line-based field sequence and (b) as point-based field sequence for the sake of consistent presentation. It can be seen that the FCO sampling fairly handles the vertical and horizontal direction, and it is preferable for

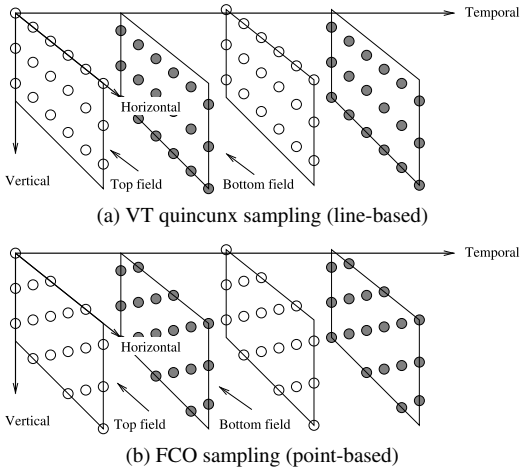

Fig. 2 Sampling formats, where the white and black circles are pixels on top and bottom fields, respectively.

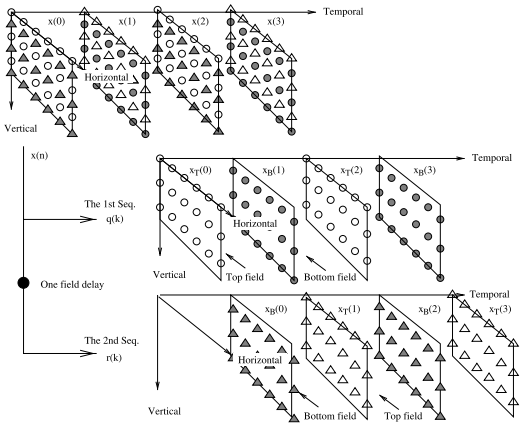

(a) VT-quincunx-based split process

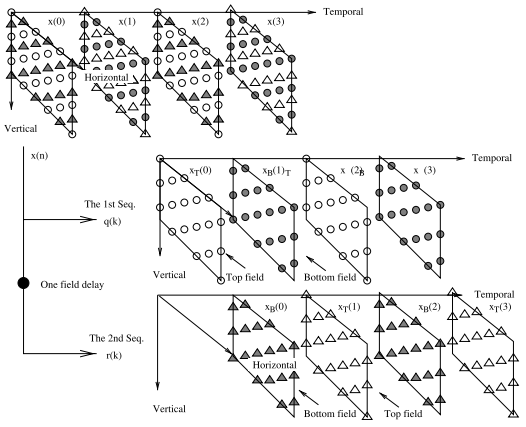

(b) FCO-based split process

Fig. 3 Field split process.

the human visual perception when compared with the VT-quincunx sampling.

2.3 Field Split Process

Figure 3(a) shows the field split process for the line-based case. In the same way, the point-based field split process can be defined as shown in Fig. 3(b) [9]. In this process, input frame sequence $x(n)$ is divided into two field sequences $q(k)$ and $r(k)$, where subscripts n and k denote the frame numbers in the full and half frame rate, respectively. In the figure, $x_{\mathrm{T}}(n)$ and $x_{\mathrm{B}}(n)$ are top and bottom fields of $x(n)$, and are associated with $q(k)$ and $r(k)$ as $q(k) = \{x_{\mathrm{T}}(2k), x_{\mathrm{B}}(2k+1)\}$ and $r(k) = \{x_{\mathrm{T}}(2k-1), x_{\mathrm{B}}(2k)\}$, respectively.

3. Equivalent Parallel Structure

The deinterlacer banks with invertible deinterlacers are shift-variant as will be shown and it was impossible to derive optimal bit-rate allocation without knowing coefficients of analysis and synthesis filters in the equivalent parallel structure. In this section, we newly drives the polyphase representation and equivalent parallel structure of a deinterlacer and reinterlacer bank. Optimal bit-rates can be calculated from the filter coefficients of the parallel structure.

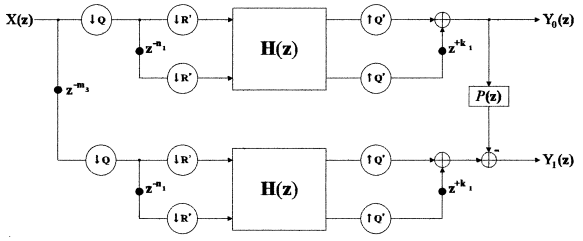

Fig. 4 Polyphase representation of a deinterlacer bank.

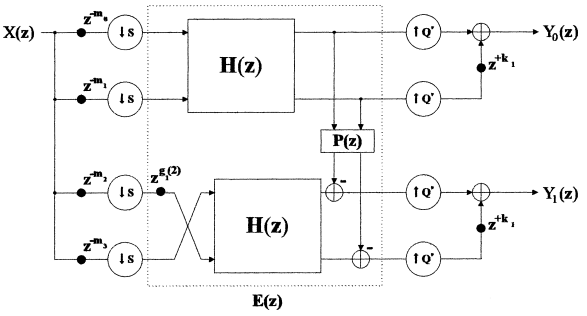

Fig. 5 Polyphase representation of a deinterlacer bank.

3.1 Deinterlacer Banks

Figure 4 shows a representation of the deinterlacer bank in terms of multidimensional multirate components, where $\mathbf{m}_3 = \begin{pmatrix}1\\0\\0\end{pmatrix}$, $\mathbf{n}_1 = \mathbf{Q}^{-1}\begin{pmatrix}1\\1\\0\end{pmatrix}$, $\mathbf{k}_1 = \begin{pmatrix}0\\1\\0\end{pmatrix}$, and the circles including $\uparrow\mathbf{Q}$, $\downarrow\mathbf{R}'$, $\downarrow\mathbf{Q}'$ denote the downsampler with a factor $\mathbf{Q}$, the downsampler with a factor $\mathbf{R}'$, and the upsampler with a factor $\mathbf{Q}'$ [13]–[15]. In this work, it is assumed that the input array $\mathbf{X}(\mathbf{z})$ is sampled on the lattice $\mathcal{L}(\mathbf{V})$ generated by the following matrix:

$$\mathbf{V} = \begin{pmatrix} P_T & 0 & 0 \\ 0 & P_V & 0 \\ 0 & 0 & P_H \end{pmatrix}, \tag{1}$$

where P_T is the temporal period between successive frames, and P_V and P_H are the vertical and horizontal sampling periods in a frame, respectively. The downsampler with factor $\mathbf{Q}$ converts the progressive scanning video $X(\mathbf{z})$ into an interlaced one. $\mathbf{H}(\mathbf{z})$ is a 3-D polyphase matrix of the invertible deinterlacer [6], [9]. $P(\mathbf{z})$ is a prediction filter. The deinterlacer bank can be expressed by the polyphase matrix from the property of multirate systems [13]. The polyphase representation is shown in Fig. 5, where $\mathbf{S} = \mathbf{QR}'$, $\mathbf{m}_i \in \mathcal{N}(\mathbf{S})$, and $\mathbf{g}_1(2) = \begin{pmatrix}-1\\0\\0\end{pmatrix}$. $\mathbf{P}(\mathbf{z})$ is a circulant matrix composed of $P(\mathbf{z})$ [13]. The whole polyphase matrix is represented as

$$\mathbf{E}(\mathbf{z}) = \begin{pmatrix} \mathbf{I} & \emptyset \\ -\mathbf{P}(\mathbf{z}) & \mathbf{I} \end{pmatrix} \begin{pmatrix} \mathbf{H}(\mathbf{z}) & \emptyset \\ \emptyset & \mathbf{H}(\mathbf{z}) \end{pmatrix} \begin{pmatrix} \mathbf{I} & \emptyset \\ \emptyset & \mathbf{JA}(\mathbf{z}) \end{pmatrix}, \tag{2}$$

where

$$\mathbf{H}(\mathbf{z}) = \begin{pmatrix} H_{\mathbf{m}_0}(\mathbf{z}) & \mathbf{z}^{-\mathbf{g}_1(1)} H_{\mathbf{m}_1}(\mathbf{z}) \\ H_{\mathbf{m}_2}(\mathbf{z}) & \mathbf{z}^{-\mathbf{g}_1(3)} H_{\mathbf{m}_3}(\mathbf{z}) \end{pmatrix}, \tag{3}$$

$$\mathbf{P}(\mathbf{z}) = \begin{pmatrix} P_{\mathbf{k}_0}(\mathbf{z}) & P_{\mathbf{k}_1}(\mathbf{z}) \\ \mathbf{z}^{-2\mathbf{Q}'^{-1}} P_{\mathbf{k}_1}(\mathbf{z}) & P_{\mathbf{k}_0}(\mathbf{z}) \end{pmatrix}, \mathbf{k}_i \in \mathcal{N}(\mathbf{Q}'), \tag{4}$$

$$\mathbf{A}(\mathbf{z}) = \begin{pmatrix} \mathbf{z}^{\mathbf{g}_1(2)} & 0 \\ 0 & 1 \end{pmatrix}, \tag{5}$$

where $\mathbf{g}_1(1) = \begin{pmatrix} 0 \\ 0 \\ 0 \end{pmatrix}$, $\mathbf{g}_1(3) = \begin{pmatrix} 0 \\ -1 \\ 0 \end{pmatrix}$. $\emptyset$, $\mathbf{I}$, and $\mathbf{J}$ are the zero, identity, and counter identity matrix, respectively. By using the following equation, this polyphase representation can be rewritten by the parallel structure shown in Fig. 6, and all of the filters are obtained as follows:

$$\begin{pmatrix} G_0(\mathbf{z}) \\ G_1(\mathbf{z}) \\ G_2(\mathbf{z}) \\ G_3(\mathbf{z}) \end{pmatrix} = \mathbf{E}(\mathbf{z}^{\mathbf{S}}) \begin{pmatrix} \mathbf{z}^{-\mathbf{m}_0} \\ \mathbf{z}^{-\mathbf{m}_1} \\ \mathbf{z}^{-\mathbf{m}_2} \\ \mathbf{z}^{-\mathbf{m}_3} \end{pmatrix}. \tag{6}$$

Examples in the case of VT-quincunx and FCO sub-sampling lattice are shown in the bellow.

3.1.1 VT-Quincunx Sub-Sampling

In the case of VT-quincunx sub-sampling, $\mathbf{Q} = \begin{pmatrix} 1 & 1 & 0 \\ -1 & 1 & 0 \\ 0 & 0 & 1 \end{pmatrix}$, $\mathbf{R}' = \begin{pmatrix} 1 & -1 & 0 \\ 1 & 1 & 0 \\ 0 & 0 & 1 \end{pmatrix}$, $\mathbf{Q}' = \begin{pmatrix} 1 & 0 & 0 \\ 0 & 2 & 0 \\ 0 & 0 & 1 \end{pmatrix}$, and $\mathbf{S} = \begin{pmatrix} 2 & 0 & 0 \\ 0 & 2 & 0 \\ 0 & 0 & 1 \end{pmatrix}$ [6]. $H_{\mathbf{m}_i}(\mathbf{z})$ is obtained as shown in the article [6, APPENDIX], and $P_{\mathbf{k}_i}(\mathbf{z})$ is given as follows:

$$P_{\mathbf{k}_0}(\mathbf{z}) = \frac{1}{2}(1 + z_T^{-1}), \tag{7a}$$

$$P_{\mathbf{k}_1}(\mathbf{z}) = 0. \tag{7b}$$

Therefore, we obtain the following filters:

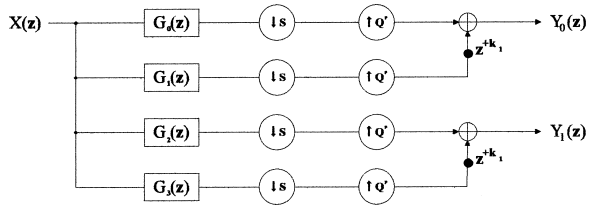

Fig. 6 Parallel composition of a deinterlacer bank.

$$G_0(\mathbf{z}) = 1, \tag{8a}$$

$$G_1(\mathbf{z}) = \frac{1}{4}z_V^2 + \frac{1}{2}z_V z_T^{-1} + \frac{1}{4}, \tag{8b}$$

$$G_2(\mathbf{z}) = -\frac{1}{2}z_T^{-2} + z_T^{-1} - \frac{1}{2}, \tag{8c}$$

$$\begin{aligned} G_3(\mathbf{z}) = &-\frac{1}{8}z_V^{-2} + \frac{1}{4}z_V^2 z_T^{-1} + \frac{1}{8}z_V^2 z_T^{-2} - \frac{1}{4}z_V z_T^{-3} \\ &+ \frac{1}{2}z_V z_T^{-2} - \frac{1}{4}z_V z_T^{-1} - \frac{1}{8}z_T^{-2} - \frac{1}{4}z_T^{-1} - \frac{1}{8}. \end{aligned} \tag{8d}$$

The amplitude responses are given in Fig. 7.

3.1.2 FCO Sub-Sampling

The similar argument holds for the case of handling the FCO sub-sampling [9]. For the FCO sampling lattice, $\mathbf{Q} = \begin{pmatrix} 1 & 1 & 0 \\ 1 & 0 & 1 \\ 0 & 1 & 1 \end{pmatrix}$, $\mathbf{R}' = \begin{pmatrix} 1 & 0 & 1 \\ 1 & 0 & -1 \\ -1 & 1 & 0 \end{pmatrix}$, $\mathbf{Q}' = \begin{pmatrix} 1 & 1 & 0 \\ -1 & 1 & 0 \\ 0 & 0 & 1 \end{pmatrix}$, $\mathbf{S} = \begin{pmatrix} 2 & 0 & 0 \\ 0 & 1 & 1 \\ 0 & 1 & -1 \end{pmatrix}$ [9]. $H_{\mathbf{m}_i}(\mathbf{z})$ is obtained as shown in Appendix B. $P_{\mathbf{k}_i}(\mathbf{z})$ is similar to the case of VT-quincunx sampling lattice. Then, the following filters are derived:

$$G_0(\mathbf{z}) = 1, \tag{9a}$$

$$G_1(\mathbf{z}) = \frac{1}{8} + \frac{1}{8}z_V z_H + \frac{1}{2}z_T^{-1} z_H + \frac{1}{8}z_V z_H^{-1} + \frac{1}{8}z_V^2 z_H^2, \tag{9b}$$

$$G_2(\mathbf{z}) = -\frac{1}{2}z_T^{-2} + z_T^{-1} - \frac{1}{2}, \tag{9c}$$

$$\begin{aligned} G_3(\mathbf{z}) = &-\frac{1}{16} - \frac{1}{16}z_T^{-2} - \frac{1}{16}z_V z_H - \frac{1}{16}z_T^{-2} z_V z_H + \frac{1}{8}z_T^{-1} \\ &+ \frac{1}{8}z_T^{-1} z_V z_H^{-1} - \frac{1}{4}z_T^{-1} z_H + \frac{1}{2}z_T^{-2} z_H - \frac{1}{4}z_T^{-3} z_H \\ &+ \frac{1}{8}z_T^{-1} + \frac{1}{8}z_T^{-1} z_V^2 - \frac{1}{16}z_V z_H^{-1} - \frac{1}{16}z_T^{-2} z_V z_H^{-1} \\ &- \frac{1}{16}z_T^{-2} z_V^2 - \frac{1}{16}z_V^2. \end{aligned} \tag{9d}$$

Since these filters are 3-D, we omit to show their amplitude responses.

3.2 Reinterlacer Banks

The polyphase representation of the reinterlacer bank can be obtained in the similar way to the deinterlacer bank. The polyphase matrix of reinterlacer bank is represented as

$$\mathbf{R}(\mathbf{z}) = \begin{pmatrix} \mathbf{I} & \mathbf{0} \\ \mathbf{0} & \mathbf{A}(\mathbf{z}^{-\mathbf{I}})\mathbf{J} \end{pmatrix} \begin{pmatrix} \mathbf{F}(\mathbf{z}) & \mathbf{0} \\ \mathbf{0} & \mathbf{F}(\mathbf{z}) \end{pmatrix} \begin{pmatrix} \mathbf{I} & \mathbf{0} \\ \mathbf{P}(\mathbf{z}) & \mathbf{I} \end{pmatrix}, \tag{10}$$

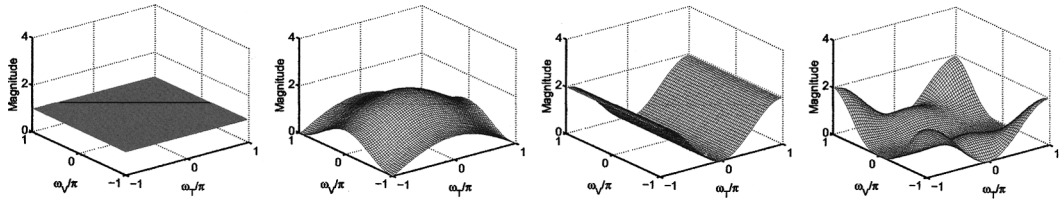

(a) $G_0(\mathbf{z})$ (b) $G_1(\mathbf{z})$ (c) $G_2(\mathbf{z})$ (d) $G_3(\mathbf{z})$

Fig. 7 Amplitude responses of filters $G_i(\mathbf{z})$.

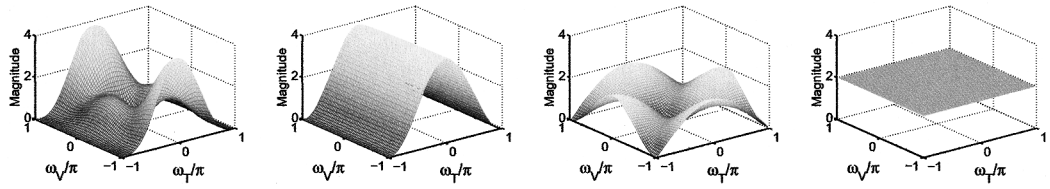

(a) $\tilde{G}_0(\mathbf{z})$ (b) $\tilde{G}_1(\mathbf{z})$ (c) $\tilde{G}_2(\mathbf{z})$ (d) $\tilde{G}_3(\mathbf{z})$

Fig. 8 Amplitude responses of filters $\tilde{G}_i(\mathbf{z})$.

where $\mathbf{F}(\mathbf{z})$ is a polyphase matrix of a reinterlacing filter:

$$\mathbf{F}(\mathbf{z}) = K\mathbf{z}^{-\mathbf{d}_F}\mathbf{I}_r(\mathbf{z})\begin{pmatrix}\mathbf{z}^{-\mathbf{g}_1(3)}H_{\mathbf{m}_3}(\mathbf{z}) & -H_{\mathbf{m}_1}(\mathbf{z}) \\ -H_{\mathbf{m}_2}(\mathbf{z}) & H_{\mathbf{m}_3}(\mathbf{z})\end{pmatrix}, \tag{11}$$

where $\mathbf{d}_F$ is delay vector and

$$\mathbf{I}_r(\mathbf{z}) = \begin{cases}\begin{pmatrix}1 & 0\\ 0 & 1\end{pmatrix}, & r = 0\\ \begin{pmatrix}0 & \mathbf{z}^{2\mathbf{R}^{r-1}\mathbf{n}_1}\\ 1 & 0\end{pmatrix}, & r = 1\end{cases} \tag{12}$$

The following filters represent the parallel structure of the reinterlacer bank.

$$\begin{pmatrix}\tilde{G}_0(\mathbf{z})\\ \tilde{G}_1(\mathbf{z})\\ \tilde{G}_2(\mathbf{z})\\ \tilde{G}_3(\mathbf{z})\end{pmatrix}^T = \begin{pmatrix}\mathbf{z}^{\mathbf{m}_0}\\ \mathbf{z}^{\mathbf{m}_1}\\ \mathbf{z}^{\mathbf{m}_2}\\ \mathbf{z}^{\mathbf{m}_3}\end{pmatrix}^T \mathbf{R}(\mathbf{z}^{\mathbf{S}}). \tag{13}$$

From these filters, optimal bit-rates can be calculated. Examples of parallel filters in the both cases of VT-quincunx and FCO sampling lattice are shown below with $K = 2$, $\mathbf{d}_F = \begin{pmatrix}1\\1\\0\end{pmatrix}$, and $r = 0$ [6].

3.2.1 VT-Quincunx Sub-Sampling

In the case of the VT-Quincunx sampling lattice, the following filters are obtained:

$$\begin{aligned}\tilde{G}_0(\mathbf{z}) &= -\frac{1}{4}z_T^{-2}z_V^{-1} - \frac{1}{2}z_T^{-1}z_V^{-1} - \frac{1}{4}z_V^{-1} + \frac{1}{2}z_T^{-1} + z_T^{-2}\\ &\quad + \frac{1}{2}z_T^{-3} - \frac{1}{4}z_V - \frac{1}{2}z_T^{-1}z_V - \frac{1}{4}z_T^{-2}z_V, \qquad (14a)\\ \tilde{G}_1(\mathbf{z}) &= 2z_T^{-1}z_V^{-1} + z_T^{-2}z_V^{-1} + z_V^{-1}, \qquad (14b)\\ \tilde{G}_2(\mathbf{z}) &= -\frac{1}{2}z_V^{-1} + z_T^{-1} - \frac{1}{2}z_V, \qquad (14c)\\ \tilde{G}_3(\mathbf{z}) &= 2z_V^{-1}. \qquad (14d)\end{aligned}$$

The amplitude responses are given in Fig. 8.

3.2.2 FCO Sub-Sampling

In the case of the FCO sampling lattice, the following filters are obtained:

$$\begin{aligned}\tilde{G}_0(\mathbf{z}) &= z_T^{-2}z_V^{-1}z_H^{-1} + \frac{1}{4}z_T^{-1}z_V^{-1}z_H^{-2} + \frac{1}{4}z_T^{-1}z_H^{-1} + \frac{1}{4}z_T^{-1}z_H^{-3}\\ &\quad + \frac{1}{4}z_T^{-1}z_Vz_H^{-2} + \frac{1}{8}z_V^{-1}z_H^{-2} + \frac{1}{8}z_H^{-1} + \frac{1}{8}z_H^{-3} + \frac{1}{8}z_Vz_H^{-2}\\ &\quad + \frac{1}{8}z_T^{-2}z_V^{-1}z_H^{-2} + \frac{1}{8}z_T^{-2}z_H^{-1} + \frac{1}{8}z_T^{-2}z_H^{-3} + \frac{1}{8}z_T^{-2}z_Vz_H^{-2}\\ &\quad + \frac{1}{2}z_T^{-1}z_V^{-1}z_H^{-1} + \frac{1}{2}z_T^{-3}z_V^{-1}z_H^{-1}, \qquad (15a)\\ \tilde{G}_1(\mathbf{z}) &= 2z_T^{-1}z_V^{-1}z_H^{-1} + z_V^{-1}z_H^{-2} + z_T^{-2}z_V^3z_H^{-2}\\ &\quad + z_T^{-1}z_V^{-2}z_H^{-2} + z_T^{-3}z_V^{-2}z_H^{-2}, \qquad (15b)\\ \tilde{G}_2(\mathbf{z}) &= \frac{1}{4}z_V^{-1}z_H^{-2} + \frac{1}{4}z_H^{-1} + \frac{1}{4}z_H^{-3}\\ &\quad + \frac{1}{4}z_Vz_H^{-2} + z_T^{-1}z_V^{-1}z_H^{-1}, \qquad (15c)\\ \tilde{G}_3(\mathbf{z}) &= 2z_V^{-1}z_H^{-2}. \qquad (15d)\end{aligned}$$

4. Performance Evaluation

In this section, we investigate the optimal bit-rate allocation by using the filter coefficients derived in Sect. 3, and then show some experimental results for evaluating the significance of the parallel representation. In this experiment, we use 450 frames of four ITE (The Institute of Image Information and Television Engineers of Japan) standard SIF video sequences; *Yachting, Whale Show, Soccer Action,* and *Crowded Cross walk*. These original sequences have a frame rate of 30 fps and a spatial resolution of 352×240.

For optimal bit-allocation, we assume to apply the entropy coded scalar quantization (ECSQ) [4, Chapter 3] to subband sequence of deinterlacer banks in the both cases of the line based and point-based system. In the followings, we compare the performance among

- Average bit allocation (no optimization),
- Frame-by-frame bit allocation through ECSQ and
- Field-by-field bit allocation through ECSQ.

The average bit allocation assigns the same average bits to every subband. Thus, it ignores the quality control. The frame-by-frame bit allocation is done by regarding the deinterlacer banks as two-channel filter banks, where $\tilde{G}_0(\mathbf{z})$ and $\tilde{G}_1(\mathbf{z})$ are considered as one filter and so $\tilde{G}_2(\mathbf{z})$ and $\tilde{G}_3(\mathbf{z})$ are. The field-by-field bit allocation is done by regarding the deinterlacer banks as four-channel filter banks. Note that in this experiment, the motion-compensation process is made inactive because the purpose is to evaluate the significance of the equivalent parallel structure.

Table 1 Energy G_b, which is just the squared norm of synthesis filter gain of bth subband.

Sub-sampling lattice	By frame		By field			
	$\|\tilde{G}_0\|^2 + \|\tilde{G}_1\|^2$	$\|\tilde{G}_2\|^2 + \|\tilde{G}_3\|^2$	$\|\tilde{G}_0\|^2$	$\|\tilde{G}_1\|^2$	$\|\tilde{G}_2\|^2$	$\|\tilde{G}_3\|^2$
	$b = 0$	$b = 1$	$b = 0$	$b = 1$	$b = 2$	$b = 3$
VT-Quincunx	8.25	5.5	2.25	6.0	1.5	4.0
FCO	9.875	5.25	1.875	8.0	1.25	4.0

Table 2 σ_b^2, the variance of bth subband in the VT-Quincunx sub-sampling case.

Video Sequence	By frame		By field			
	$b = 0$	$b = 1$	$b = 0$	$b = 1$	$b = 2$	$b = 3$
Yachting	4082.7	58.426	4170.0	4033.9	85.196	31.656
Whale Show	1723.1	357.63	1953.6	1522.1	521.43	193.82
Soccer Action	1665.9	183.07	1823.6	1542.5	280.28	85.861
Crowded Crosswalk	2423.5	223.7	2581.0	2275.1	347.9	99.642

Table 3 σ_b^2, the variance of the bth subband in the FCO sub-sampling case.

Video Sequence	By frame		By field			
	$b = 0$	$b = 1$	$b = 0$	$b = 1$	$b = 2$	$b = 3$
Yachting	4105.9	53.952	4163.3	4086.0	85.346	22.559
Whale Show	1734.0	322.67	1950.4	1549.3	521.53	123.80
Soccer Action	1674.3	170.01	1815.2	1566.7	279.06	60.957
Crowded Crosswalk	2437.3	217.62	2574.8	2311.3	347.59	87.653

4.1 Entropy Coded Scalar Quantization (ECSQ)

Let us explain the method of the quantization applied to the optimal bit allocation in this experiment. The optimal rates R_b for each subband can be obtained from the following expression:

$$R_b = R + \frac{1}{2}\log_2 \frac{G_b W_b \epsilon_b^2 \sigma_b^2}{\prod_{l=0}^{B-1}(G_l W_l \epsilon_l^2 \sigma_l^2)^{\eta_l}}, \tag{16}$$

where b is subband index, B is the number of subbands, G_b is the synthesis gain associated with band b, W_b is the weighted MSE, σ_b^2 is a variance of each subband, and R is an average rate of all subbands [4, Chapter 5], we have selected $\epsilon_b^2 = 1$ by assuming IID Gaussian data. The optimal bit-rate R_b is calculated by using the synthesis gains G_b and subband variances σ_b^2 shown in Tables 1, 2, and 3. Quantization steps of each subband is derived as follows:

$$\Delta_b = \sqrt{\frac{\epsilon_b^2 \sigma_b^2}{c_b}} 2^{-R_b}, \tag{17}$$

where $c_b = 1/12$ for ECSQ [4, Chapter 3]. The procedure of ECSQ is defined as:

$$q = \begin{cases} \mathrm{sign}(x)\lfloor \frac{|x|}{\Delta} + \xi \rfloor, & \frac{|x|}{\Delta} + \xi > 0 \\ 0, & \text{otherwise} \end{cases} \tag{18}$$

where $\mathrm{sign}(x)$ is a function returns the sign of x. The reconstruction procedure is defined as

$$\hat{x}_q = \begin{cases} 0, & q = 0 \\ \mathrm{sign}(q)(|q| - \xi + \delta)\Delta, & q \neq 0 \end{cases} \tag{19}$$

In this paper, we select $\xi = 0$, and $\delta = 1/2$ [4, Chapter3].

4.2 Discussion

The average PSNR results for the line- and point-based system are shown in Figs. 9 and 10, respectively. Let us summarize the results below.

- It is seen that the optimization techniques improve the PSNR from 2.0 dB to 10.0 dB from about the average bit-rate allocation with no-optimization.
- The field-based optimization roughly shows a superior performance to the frame-based one. This is because the field-based procedure more finely derives the optimal rate than the frame-based one through the theoretical analysis of deinterlacer banks.
- The FCO sub-sampling system numerically shows better performance than the VT-quincunx system in terms of PSNR, where the differences range from 0.2 dB to 0.5 dB and are too small to see from the graphs.

From the first and second points, it is verified that our analysis of the deinterlacer banks are very useful for further investigation of rate-distortion control techniques and the above results are very incentive to proceed the analysis when some motion-compensation technique is applied. Note that the frame-based procedure is simpler than, but well approximates the field-based one. This paper showed that deinterlacer banks can be represented by shift-varying systems and newly derived the equivalent parallel structure. Finally, it was shown that the optimal bit-rate allocation become possible.

5. Conclusions

In this paper, we derived an equivalent parallel structure of deinterlacer bank and reinterlacer banks. Then, we applied the equivalent structure to optimal bit-rate allocation by using the synthesis filter coefficients of the reinterlacer bank. Some experimental results showed the effectiveness of the optimal bit-rate allocation through our analysis, and the significance of the analysis was verified.

Acknowledgment

This work was in part supported by the Grand-in-Aid for Scientific Research No.16-5404 from Society for the Promotion of Science and Culture of Japan, and the Grand-in-Aid for Scientific Research from the UNIONTOOL Scholarship Foundation.

References

[1] J.R. Ohm, "Three-dimensional subband coding with motion compensation," IEEE Trans. Image Process., vol.3, no.5, pp.559–571, Sept. 1994.

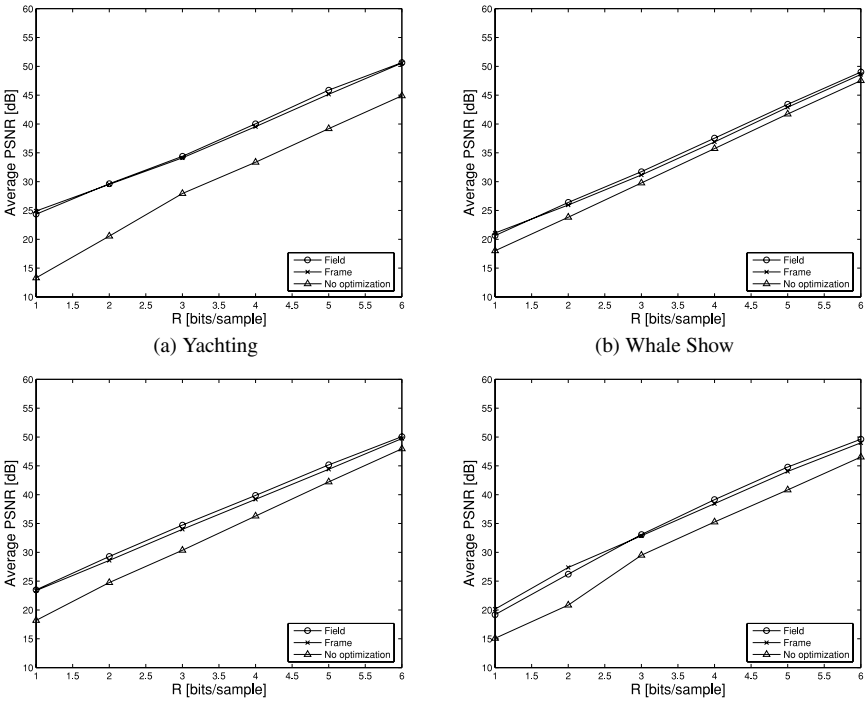

(a) Yachting (b) Whale Show

(c) Soccer Action (d) Crowded Crosswalk

Fig. 9 VT-quincunx sub-sampling (line-based) case. 'Frame' and 'Field' denote optimization by frame and by field, respectively.

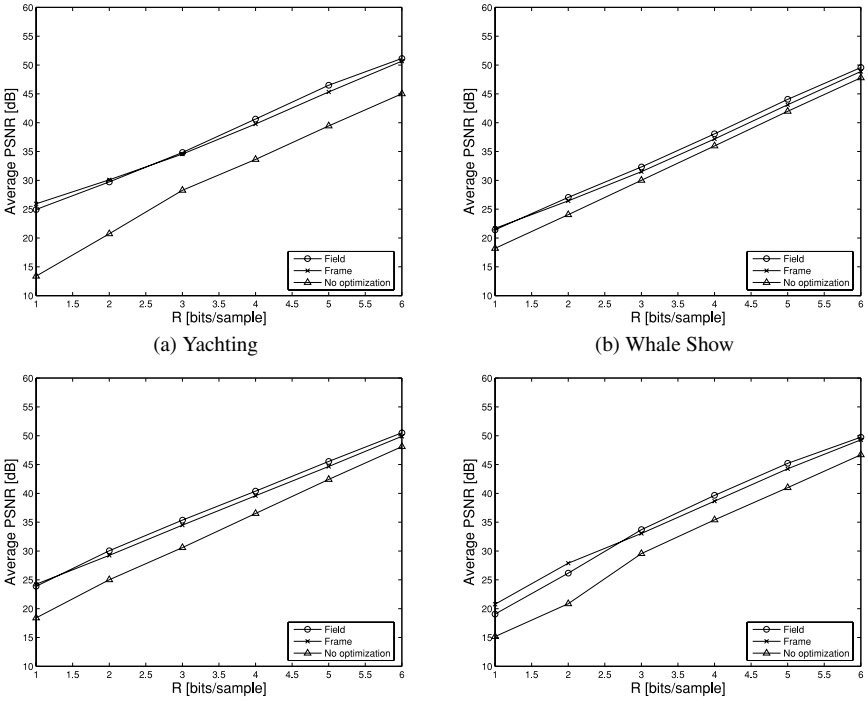

(a) Yachting (b) Whale Show

(c) Soccer Action (d) Crowded Crosswalk

Fig. 10 FCO sub-sampling (point-based) case. 'Frame' and 'Field' denote optimization by frame and by field, respectively.

[2] A. Secker and D. Taubman, "Lifting-based invertible motion adaptive transform (LIMAT) framework for highly scalable video compression," IEEE Trans. Image Process., vol.12, no.12, pp.1530–1542, Dec. 2003.

[3] N. Mehrserest and D. Taubman, "Adaptively weighted update steps in motion compensated lifting based scalable video compression," Proc. IEEE Int. Conf. Image Processing, pp.771–774, Barcelona, Spain, Sept. 2003.

[4] D.S. Taubman and M.W. Marcellin, JPEG2000: Image Compression Fundamentals, Standards and Practice, Kluwer Academic Pub., 2002.
[5] Standard Codecs: Image Compression to Advanced Video Coding, The IEE, 2003.
[6] S. Muramatsu, T. Ishida, and H. Kikuchi, "Invertible deinterlacing with sampling-density preservation: Theory and design," IEEE Trans. Signal Process., vol.51, no.9, pp.2343–2356, Sept. 2003.
[7] H. Kikuchi, S. Muramatsu, and T. Ishida, "Reversible conversion between interlaced and progressive scan formats and its efficient implementation," Proc. EUSIPCO, no.448, Toulouse, France, Sept. 2002.
[8] S. Muramatsu, T. Ishida, and H. Kikuchi, "Perfect reconstruction deinterlacer banks for field scalable video compression," Proc. IEEE Int. Conf. Image Processing, pp.2279–2282, Singapore, Oct. 2004.
[9] D. Kitagawa, T. Ishida, S. Muramatsu, and H. Kikuchi, "Maximally-decimated perfect reconstruction deinterlacer banks based on FCO-sampling," Proc. ITC-CSCC, no.7BIL-3, Sendai, Japan, July 2004.
[10] T. Ishida, S. Muramatsu, D. Kitagawa, J. Uchita, M. Hiki, and H. Kikuchi, "Performance evaluation of spatio-temporal multi-resolution analysis with deinterlacer banks," Proc. SPIE, Visual Commun. Image Process., pp.177–188, July 2005.
[11] T. Ishida, S. Muramatsu, J. Uchita, D. Kitagawa, and H. Kikuchi, "Spatio-temporal multi-resolution analysis through hierarchical deinterlacer banks," Proc. IWAIT, pp.139–144, Jeju, Korea, Jan. 2005.
[12] S.J. Choi and J.W. Woods, "Motion-compensated 3-d subband coding of video," IEEE Trans. Image Process., vol.8, no.2, pp.155–167, Feb. 1999.
[13] P.P. Vaidyanathan, Multirate Systems and Filter Banks., Englewood Cliffs, NJ, Prentice-Hall, 1993.
[14] T. Chen and P.P. Vaidyanathan, "Recent developments in multi-dimensional multirate systems," IEEE Trans. Circuits Syst. Video Technol., vol.3, no.2, pp.116–137, April 1993.
[15] T. Chen and P.P. Vaidyanathan, "The role of integer matrices in multidimensional multirate systems," IEEE Trans. Signal Process., vol.3, no.2, pp.116–137, 1993.

Appendix A: Notations

D The number of dimensions.
N Set of all $D \times 1$ integer vectors.
$\mathbf{z}$ $D \times 1$ integer vector that consists of variables in a D-dimensional z-domain, that is, $\mathbf{z} = (z_0, z_1, z_2, \ldots, z_{D-1})^T$. For 3-D progressive arrays, z_0, z_1, and z_2 denote the variables for the temporal, vertical, and horizontal directions, respectively. For these arrays, we express $\mathbf{z}$ as $\mathbf{z} = \begin{pmatrix} z_T \\ z_V \\ z_H \end{pmatrix}$.
$\mathbf{z^n}$ Product defined by $\mathbf{z^n} = z_0^{n_0} z_1^{n_1} z_2^{n_2} \ldots z_{D-1}^{n_{D-1}}$, where $\mathbf{n}$ is a $D \times 1$ integer vector, and n_k denotes the k-th element of $\mathbf{n}$.
$\mathcal{L}(\mathbf{V})$ Set of all vectors of the form $\mathbf{Vn}$, $n \in \mathcal{N}$.
$\mathcal{N}(\mathbf{Q})$ Set of integer vectors of the form $\mathbf{Qx}$, $\mathbf{x} \in [0,1)^D$, where $[0,1)^D$ is the set of $D \times 1$ real vectors $\mathbf{x}$ with components x_i in the range $0 \le x_i < 1$.

Appendix B: Proof of the PR Property

Here, let us prove the invertibility of the proposed deinterlacing filter. As a preliminary, suppose we have the following filter as shown in [6, Theorem 1] Fig. (A· 1):

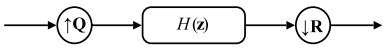

Fig. A· 1 Sampling lattice converter.

$$H(\mathbf{z}) = 1 + h(1,0,0)z_T^{-1} + h(0,1,0)(z_V^1 + z_V^{-1}) + h(0,0,1)(z_H^1 + z_H^{-1}) \quad (\text{A}\cdot 1)$$

To evaluate the filter by using the theorem shown in [6], we decompose the filter into four polyphase components as follows:

$$\mathbf{H}(\mathbf{z}) = \sum_{k=0}^{3} \mathbf{z}^{-\mathbf{m}_k} H_{\mathbf{m}_k}(\mathbf{z}^{\mathbf{S}}), \mathbf{m}_k \in \mathcal{N}(\mathbf{S}), \quad (\text{A}\cdot 2)$$

where $\mathbf{m}_0 = (0,0,0)^T$, $\mathbf{m}_1 = (1,1,0)^T$,$\mathbf{m}_2 = (0,1,0)^T$ and $\mathbf{m}_3 = (1,0,0)$, and $\mathcal{N}(\mathbf{S})$ denotes the set of integer vectors given by $\mathbf{Sx}$ for the set of 3×1 real vectors $\mathbf{x}$ with components x_i in the range $0 \le x_i < 1$ for a 3×3 non-singular integer matrix $\mathbf{S}$.

It can be verified that the filter can be represented by

$$\begin{aligned}\mathbf{H}(\mathbf{z}) =& \mathbf{z}^{\mathbf{S}\begin{pmatrix}0\\0\\0z\end{pmatrix}} \cdot \mathbf{z}^{-\mathbf{m}_0} + 0 \cdot \mathbf{z}^{-\mathbf{m}_1} + \left\{ h(0,1,0)\left(\mathbf{z}^{\mathbf{S}\begin{pmatrix}0\\1\\1\end{pmatrix}} + 1 \right) \right. \\ & \left. + h(0,0,1)\left(z^{\mathbf{S}\begin{pmatrix}0\\1\\0\end{pmatrix}} + z^{\mathbf{S}\begin{pmatrix}0\\0\\1\end{pmatrix}} \right) \right\} \mathbf{z}^{-\mathbf{m}_2} \\ & + h(1,0,0)\mathbf{z}^{\mathbf{S}\begin{pmatrix}0\\0\\0\end{pmatrix}} \cdot \mathbf{z}^{-\mathbf{m}_3}. \end{aligned} \quad (\text{A}\cdot 3)$$

Thus, we have the following relations:

$$H_{\mathbf{m}_0} = 1 \quad (\text{A}\cdot 4\text{a})$$
$$H_{\mathbf{m}_1} = 0 \quad (\text{A}\cdot 4\text{b})$$
$$H_{\mathbf{m}_2} = h(0,1,0)\left(\mathbf{z}^{\begin{pmatrix}0\\1\\1\end{pmatrix}} + 1 \right) + h(0,0,1)\left(\mathbf{z}^{\begin{pmatrix}0\\1\\0\end{pmatrix}} + \mathbf{z}^{\begin{pmatrix}0\\0\\1\end{pmatrix}} \right) \quad (\text{A}\cdot 4\text{c})$$
$$H_{\mathbf{m}_3} = h(1,0,0) \quad (\text{A}\cdot 4\text{d})$$

According to [6], let us check if the determinant of the following polyphase matrix is a monomial in $\mathbf{z}$. Substituting Eqs. (A· 4) into (3), we have

$$\det\mathbf{H}(\mathbf{z}) = h(1,0,0) \cdot \mathbf{z}^{-\begin{pmatrix}0\\1\\0\end{pmatrix}} \quad (\text{A}\cdot 5)$$

Since the determinant is a monomial in $\mathbf{z}$, the filter shown in Eq. (A· 1) provides an FIR invertible deinterlacer.

Minoru Hiki received B.E. degree from Niigata University, Niigata, in 2005. He is currently the candidate for the M.E. degree at Niigata University. His research interests are in digital signal processing, image/video processing, and video coding. He is a student member of IEEE (Institute of Electrical and Electronics Engineers, Inc.).

Shogo Muramatsu received B.E., M.E., and D. Eng. degrees in electrical engineering from Tokyo Metropolitan University in 1993, 1995, and 1998, respectively. From 1997 to 1999, he worked at Tokyo Metropolitan University. In 1999, he joined Niigata University, where he is currently an associate professor of Electrical and Electric Engineering, Faculty of Technology. During year from 2003 to 2004, he was a visiting scientist at University of Florence, Italy. His research interests are in digital signal processing, multirate systems, image processing and VLSI architecture. Dr. Muramatsu is a member of IEEE (Institute of Electrical and Electronics Engineers, Inc.), IPSJ (Information Processing Society of Japan), ITE (Institute of Image Information and Television Engineers), and IIEEJ (Institute of Image Electronics Engineers).

Takuma Ishida received B.E., M.E., and Dr. Eng. degrees from Niigata University, Japan, in 2001, 2003 and 2006, respectively. From 2004 to 2006, he was a research fellow of the Japan Society for the Promotion of Science (JSPS Research Fellow). From 2006 he works at Product Development Department, NETCLEUS Systems corporation. His research interests are in digital signal processing, image/video processing and VLSI architecture as well as wireless communication systems. Dr. Ishida is a member of the IEEE (Institute of Electrical and Electronics Engineers, Inc.).

Hisakazu Kikuchi received B.E. and M.E. degrees from Niigata University, Niigata, Japan, in 1974 and 1976, respectively, and Dr. Eng. degree in electrical and electronic engineering from Tokyo Institute of Technology, Tokyo, Japan in 1988. From 1976 to 1979 he worked at Information Processing Systems Laboratory, Fujitsu, Ltd., Tokyo. Since 1979 he has been with Niigata University, where he is a Professor at Department of Electrical Engineering. During a year of 1992 to 1993, he was a visiting scientist at the California, Los Angeles. His research interests include digital signal processing, image/video processing, and wavelets as well as spread spectrum communication systems. Dr. Kikuchi is a member of IEEE (Institute of Electrical and Electronics Engineers), ITE (Institute of Image Information and Television Engineers of Japan), and Japan Society for Industrial and Applied Mathematics, Research Institute of Signal Processing, and SPIE.